Title: Sustaining the cell energy in dynamic environments requires photosynthetic electron flows with diverse bandwidths

Authors: Sai Kiran Madireddi[1,$], Liat Adler[1,2,$], Carolyne Stoffel[1,$], Myria Schröder[1], Dimitri Tolleter[1], Adrien Burlacot[1,3*]

Affiliations:

[1]Biosphere Science and Engineering Division, Department of Plant Biology, Carnegie Science, Stanford, CA, 94305 USA

[2]Department of Bioengineering, Stanford University, Stanford, CA, 94305, USA

[3]Department of Biology, Stanford University, Stanford, CA, 94305, USA

[$] These authors contributed equally to this study

[*]corresponding author: A.B., aburlacot@carnegiescience.edu

ORCID IDs: 0000-0002-1820-1033 (S.K.M.), 0000-0002-4839-418X (L.A.), 0000-0002-4078-6250 (C.S.), 0009-0004-5757-9209 (M.S.) 0000-0003-1214-3140 (D.T.), 0000-0001-7434-6416 (A.B.)

Author contributions: A.B. designed, led, and coordinated the research; S.K.M., L.A., M.S., C.S., D.T., and A.B. performed experiments; A.B. made figures with help from L.A. and C.S.; A.B. developed the analytical framework; A.B., L.A., S.K.M., and D.T. analyzed data; AB wrote the paper with inputs from all authors.

Abstract

All living cells depend on the dynamic balance between their energy supply and demand to survive and thrive in dynamic environments. In extreme cases, like for photosynthetic organisms, their energy source, light, can fluctuate dramatically in intensity over timescales of seconds to hours. While various photosynthetic electron flows (EF) are crucial for maintaining bioenergetic homeostasis, how EFs are modulated to respond to dynamic energy intake remains unclear. Here, we show in the model green alga *Chlamydomonas reinhardtii* that each EF is best suited to a specific domain of energetic fluctuation periodicity for which it can support the cell's energetic needs, which we term bandwidth. By systematically exposing cells to a range of light periodicities, we show that while cyclic EF has a large bandwidth, pseudo-cyclic EF (PCEF) can only sustain the cell's energetic needs for fast light fluctuations, and that the interplay between the chloroplast and the mitochondria (CMEF) has a limited bandwidth. We further show that the bandwidths of PCEF and CMEF, specialized for dynamic lights, are related to their capacity to generate ATP and protect the photosynthetic apparatus. Finally, we show that in wild-type cells, the activity level of PCEF and CMEF matches their bandwidth, and we propose that cells tune the relative activity of each AEF depending on the light fluctuation frequency. Our work opens an avenue of research to characterize the molecular mechanisms required for phototrophic growth in complex and dynamic energetic landscapes. It further provides a generalizable framework for understanding the physiological importance of molecular mechanisms in a dynamic environment.

Introduction

Life depends on extracellular energy to support growth, reproduction, and survival. However, the availability of energetic vectors (i.e., organic carbon, light, reductant) is variable. It fluctuates over a wide range of timescales, with energetic overload or starvation often lasting anywhere from milliseconds to hours, days, or months (*1*, *2*). Consequently, cells must dynamically manage their cellular energy in response to these changes. Electron flows (**EFs**), active in energetic organelles such as the mitochondria or chloroplasts in eukaryotes, play a central role in cellular health by dynamically balancing cellular energy demand and supply (*3*). EFs dynamically poise ATP and redox levels in the cell by coupling electron transport with proton translocation across membranes, hence maintaining the bioenergetic homeostasis. Impairments of EFs strongly affect bioenergetic homeostasis and have been linked with aging (*4*) and multiple human diseases (*5–7*), including chronic fatigue (*8*) or long COVID-19 (*9*), and cause reduced fitness across all taxa, including yeast (*10*), nematodes (*11*), plants (*12*, *13*), or algae (*14*, *15*). While EFs' flexibility has been proposed to be critical in modulating the cell's bioenergetic homeostasis in response to variable energetic availability, how this flexibility is managed remains unclear.

Photosynthetic organisms, like plants or algae, are particularly subject to dynamic energy input since multiple natural factors like canopy movement, clouds, or water mixing dynamically change the amount of light energy available on timescales ranging from milliseconds to hours (*2*, *16*). Light intensity variations span a large magnitude of intensities from low, limiting light to intense, over-saturating light (*17*). In the chloroplasts of plants and eukaryotic algae, absorbed light energy is used by photosystems (**PS**) I and II to generate a linear electron flow (**LEF**) that produces NADPH and drives ATP synthesis by producing a trans-thylakoidal proton gradient (**Fig. 1A**), both of which support the energetic needs of CO_2 conversion to biomass. However, LEF cannot sustain the cell's energy by itself (*12*, *15*), and alternative electron flows (**AEF**) are required to balance the ATP needs and control photosynthetic electron transport by translocating additional protons across energized membranes in response to light (**Fig. 1A**). Those include (*i*) cyclic electron flow (**CEF**), which recycles reductant around PSI (*18*), (*ii*) pseudo-cyclic electron flow (**PCEF**), which reduces O_2 into H_2O downstream of PSI (*19–21*) and (*iii*) chloroplast to mitochondrial electron flow (**CMEF**) which involves the translocation of reductant produced by

PSII to the mitochondria (*14*, *22–24*) (**Fig. 1A**). In the model green microalgae *Chlamydomonas reinhardtii* (*Chlamydomonas* hereafter), CEF, PCEF, and CMEF are the main AEFs sustaining photosynthesis under continuous illumination (*15*). The main pathway of CEF is regulated by the proton gradient regulation-like 1 (**PGRL1**; **Fig. 1A**) (*25*), and PCEF is mediated by flavodiiron proteins (**FLVs**; **Fig. 1A**)(*21*). While the molecular mechanisms involved in redox exchange between the chloroplast and the mitochondria for CMEF remain to be discovered (*26*, *27*), the majority of CMEF is mediated through the respiratory complex III (*15*) (**Fig. 1A**). Mutants impaired in CEF have been reported to be sensitive to high light and some fluctuating light (*28*, *29*). PCEF is particularly important during dark-to-light transition (*21*, *24*), and CMEF has been proposed to mostly act as a long-term electron valve (*30*). While maintaining energetic homeostasis requires some interplay between CEF, PCEF, and CMEF (*16*, *24*), how this interplay proceeds in a dynamic light environment remains unresolved.

In this work, we employed CRISPR Cas9-guided mutagenesis and chemical inhibition of the mitochondrial complex III to generate mutants that rely solely on one AEF to support LEF. We first used these strains to characterise the importance of each AEF in maintaining LEF and growth under various light intensities. We then developed an approach inspired by frequency-domain analysis to define, for each AEF, the bandwidths of light intensity fluctuation periodicities (referred hereafter simply as periodicities) for which it can sustain LEF to power at least 50% of the wild-type growth. We use this method to show that while PCEF has a bandwidth limited to periodicities shorter than a few minutes, CEF harbors a broad bandwidth across all the periodicities tested, and CMEF has a bandwidth centered around periodicities of 10 minutes. We show that the bandwidth of PCEF and CMEF reflects their capacity to sustain and protect photosynthesis in response to the first few hours of dynamic light. We further reveal that in wild-type cells acclimated to various light periodicities, the activities of PCEF and CMEF mirror their characterized bandwidth. Finally, we propose that cells regulate the mix of AEFs they use to optimize it for the periodicity of light change.

Results

Each AEF's capacity to maintain energetic homeostasis depends on light intensity and exposure duration.

When two of the three main AEFs are inhibited, the third one is the only one supporting LEF in rebalancing the energetic needs of photoautotrophic cells (*15*). To impair CEF and PCEF, we used CRISPR Cas9-guided mutagenesis to generate insertional mutants impaired in the accumulation of PGRL1 (***pgrl1***, impaired in CEF), FLVB (***flvB***, impaired in PCEF), or both (***pgrl1 flvB***), all in the same CC125 genetic background (**WT**) (**Fig. S1**). To isolate the capacity of each AEF in supporting growth and photosynthesis, we combined these mutants along with the respiratory complex III inhibitor myxothyazol (**myxo**), which inhibits CMEF (*31*) (**Fig. 1B** illustrates mutants/conditions for which each AEF is solely active). We first tested the capacity of each AEF in sustaining growth for different light intensities in the presence or absence of myxo (**Fig. 1B; Fig. S2**). When only CMEF was active, cells grew less than the WT under medium (**ML**) and high (**HL**) light but grew indistinguishably from the WT under low light (**LL**) (*pgrl1 flvB* mutants, **Fig. 1B, Fig. S2**). When only CEF was active, cells grew as well as the WT for all light intensities (*pgrl1+myxo*, **Fig. 1B, Fig. S2**). However, when only PCEF was active, cells were susceptible to increasing light intensity (*flvB+myxo*, **Fig. 1B, Fig. S2**). To assess if the growth differences observed were linked with the capacity of each AEF to sustain photosynthesis, we measured the electron transport rate (**ETR**) through PSII in response to a stepwise increase in light intensity (**Fig. 1C; Fig. S3**). When only CMEF is active, WT levels of ETR are sustained under LL, but a marked decrease of ETR is observed with increasing light intensities (**Fig. 1C; Fig. S3**). However, when either PCEF or CEF are active, between 30% and 60% of the WT ETR is sustained for most light intensities (**Fig. 1C, Fig. S3**). We conclude from these experiments that CMEF can sustain full photosynthetic activity and long-term growth only under LL. Interestingly, the discrepancy between the amount of short-term photosynthesis (**Fig. 1C**) and long-term growth (**Fig. 1B**) sustained by PCEF and CEF under HL reveals that while PCEF can only sustain substantial photosynthetic activity for short timescales, CEF likely operates best at long timescales to sustain WT levels of photosynthesis.

PCEF and CMEF bandwidths are specialized for dynamic light conditions.

Besides intensity, a key parameter that characterizes dynamic light intensities is how frequently light shifts from high to low intensities (*17*, *32*). To better capture the functional domain of importance for each AEF under dynamic light intensities, we used a method inspired by frequency-domain analysis, which involves measuring AEF activity and importance relative to

the periodicity of a periodic light fluctuation. We first assessed the growth of strains treated and untreated with myxo in response to periodic HL/darkness shifts (**Fig. 2A**) for light periodicities ranging from one minute to four hours (**Figs. S4, S5**); continuous HL, and ML delivering the same average light energy as the fluctuating light were used as controls. As expected, when all AEF are inactive, cells do not grow for any light periodicity (*pgrl1 flvB* +myxo, **Figs. S4, S5**). We quantified the growth of mutants on solid media relative to the WT from the same plate (**Figs. S4, S5)** to estimate the relative gross loss of each mutant (**Fig. S6**). We used this data to assess the relative growth sustained when only CMEF, PCEF, or CEF are active (**Fig. 2B**). By defining the bandwidth of an AEF as being the periodicity range for which, when it is the main AEF active, it can sustain more than 50% of the WT's growth, we conclude that while CEF has a large bandwidth, sustaining growth for all periodicities tested (**Fig. 2B**), PCEF has a "high-pass" bandwidth, with substantial growth capacity sustained for periodicities lower than 10 minute (**Fig. 2B**). Surprisingly, CMEF shows a "passband" bandwidth centered around a 10 minute periodicity (**Fig. 2B**). We conclude from this experiment that while CEF can balance the cell's energy under continuous light and for most periodicities of dynamic light, PCEF and CMEF exhibit bandwidths that make them specialized for dynamic light conditions, albeit focused on different periodicities.

PCEF and CMEF bandwidths are related to their capacity to sustain and protect photosynthesis in a dynamic light regime.

AEFs contribute to the energetic balance by both (i) producing ATP and (ii) establishing a proton gradient which induces mechanisms protecting the photosynthetic electron transport system (*24*, *33*). To further explore which of these mechanisms might be the most prominent for the dynamic-light-specific AEFs, we tested the ability of PCEF and CMEF to sustain LEF and maintain active PSII. We measured the ETR to assess LEF and Fv/Fm, which is a chlorophyll fluorescence parameter relative to the maximal PSII efficiency as a proxy for PSII degradation after exposure to 4 hours of HL, either continuous or fluctuating (**Fig. 3, Fig. S7**). When only CMEF was active, a slight decrease in Fv/Fm was observed for all light treatments (**Fig. 3A, Fig. S7**), suggesting that protecting PSII from inhibition does not explain the bandwidth of CMEF. Conversely, CMEF only maintained 30% of WT ETR levels under continuous HL, up to 70% for periodicities between 2 and 120 minutes, and dropped to 50% of WT levels for a periodicity of 1

min (**Fig. 3A**). This suggests that the bandwidth of CMEF is mainly dictated by the limited capacity of CMEF to produce ATP during continuous HL and short periodicities. On the other hand, when only PCEF is active, the Fv/Fm is drastically reduced at HL compared to the WT and increases with shorter periodicities of light (**Fig. 3B, Fig. S7**), a similar trend being observed at the ETR level (**Fig. 3B, Fig. S7**). This suggests that the bandwidth of PCEF is dictated by the limited capacity of PCEF to translocate protons during long periodicities of light, to both produce ATP and activate PSII protection mechanisms. We conclude from this experiment that while the CMEF bandwidth mainly follows its ATP production capacity, the PCEF bandwidth is dictated by both its ATP production and photoprotection capacity.

Cells respond to the periodicity of light by activating the most relevant AEF.

Given that CMEF and PCEF have bandwidths tailored for dynamic light, we hypothesized that their activity in WT cells is influenced by light periodicity to optimize AEFs' capacities. Since both CMEF and PCEF are consuming O_2, we used a membrane inlet mass spectrometer to measure O_2 exchange rates in WT cells acclimated to various periodicities of light. To assess PCEF, we measure the transient O_2 uptake rates at the onset of a dark-to-light transition (**Fig. 4A, Fig. S8**), which reflects mainly PCEF (*21*). Periodicities of light shorter than 10 minutes led to an increase in the transient O_2 uptake in response to light (**Fig. 4A**); this increase was paralleled by a higher protein level of both proteins mediating PCEF for short periodicities than for long periodicities (FLVA and FLVB, **Fig. S9**). We measured respiration in the dark as a proxy for CMEF, while continuous HL and a periodicity of one minute showed similar levels of dark O_2 uptake, periodicities ranging from 10 to 120 minutes showed increased dark O_2 uptake rates, with a maxima reached for 10 minute periodicity (**Fig. 4B**). We conclude from these experiments that WT cells acclimate to the light periodicity that they are subject to by activating the AEF with the most relevant bandwidth.

Discussion

Light energy availability is one of the most dynamic conditions found in the environment, with arguably the most diverse patterns, with changes happening at timescales ranging from milliseconds to days (*2*). Despite the early discovery by Garner and Allard that plant productivity depends largely on how dynamic light is (*34*), how key characteristics of light dynamics

influence the molecular mechanism involved remains unclear (*17*). Here, we show that light periodicity is a major parameter defining the molecular mechanisms used in the green microalgae *Chlamydomonas* (**Figs 2-4**). Among the three main AEFs that maintain the bioenergetic homeostasis in response to light, PCEF and CMEF harbor bandwidths of physiological importance specific to short and medium periodicities of light, respectively (**Fig. 2**). We reveal that the level of activity of PCEF and CMEF in WT cells acclimated to various periodicities of light parallels their bandwidth (**Fig. 4**), suggesting that photosynthetic cells sense the periodicity of light to use the most relevant AEF. Interestingly, measurements shown in **Fig. 4** are performed 15 minutes after cells are extracted from their dynamic light environment; hence, our results further suggest that the periodicity-specific acclimation involves long-term changes induced by each periodicity. For PCEF, it is clear that the decreasing amount of FLVs proteins (**Fig. S9**) explains the low activity of PCEF under continuous light and long periodicities of light, potentially due to increased degradation of FLV proteins. However, FLVs amounts for one-minute and 10-minute periodicities are similar, suggesting a role of post-transcriptional modifications, like the thiol-based reduction of FLVA (*35*), might be involved in enhancing PCEF capacity when short periodicities are sensed.

The bandwidths of PCEF and CMEF qualitatively match their capacity to maintain LEF (**Fig. 3**) and their activation level in WT cells acclimated to each periodicity of light. However, there are some quantitative differences, which likely reflect at least two effects: (i) small imbalances created by the mutation/inhibitor add up over time and could lead to more drastic long-term effects than short-term effects as seems to be the case when only CMEF is active (**Figs. 2B; 3A and 4B**) (ii) strong imbalances created by the mutation/inhibitor might take more time to be compensated for on long timescales by metabolic adjustments, as seems to be the case when only PCEF is active (**Figs. 2B; 3B and 4A**). The quantitative differences might also stem from variation in the culture condition (liquid vs solid), which could have impacted the amount of HL perceived. Overall, similar qualitative behaviors of the capacity of either CMEF or PCEF to support various parameters relative to periodicities of light point to the bioenergetic importance of PCEF and CMEF being for short and medium periodicities of dynamic light, respectively.

PCEF's bandwidth may reflect the molecular mechanism of FLVs.

Since the measurement of PCEF *in vivo* by Radmer and Kok (*36*) and the later description of the role of FLVs in PCEF (*20*, *21*), the role of PCEF has mostly been seen as a transient AEF active mainly during the first minute of dark-to-light transients. Here, we reveal that while PCEF still can sustain photosynthesis for illumination times longer than 10 minutes (**Fig. 1C**), it cannot sustain long-term photosynthesis and growth for continuous HL (**Fig. 1B**) or long periodicities of light (**Fig. 2B**). This is likely due to degradation of FLV proteins over long timescales of HL (**Fig. S9**). PCEF is efficient at generating a trans-thylakoidal proton gradient (*15*, *21*, *37*) by safely producing H_2O (*38*), and FLVs are particularly good at taking electrons (*39*), it is therefore surprising that PCEF is mainly active for short light periodicities or during light transients and cannot sustain cells' bioenergetics during long phases of continuous illumination. The catalytic mechanism of FLVs is not fully resolved (*40*), but experiments have shown that FLVs from the anaerobic bacteria *Syntrophomonas wolfei* produce H_2O_2 when using NADPH as an electron donor (*41*)). While FLVs in phototrophs likely use ferredoxins as their main electron donor (*42*), they can also use NADPH as an electron donor (*43*). Ferredoxin is reduced quickly by PSI upon illumination, but $NAPD^+$ takes time to be reduced to NADPH by the Ferredoxin-NADP reductase; hence, NADPH levels often increase with time of illumination (*44*), and steady-state levels of NADPH are positively correlated with light intensity (*45*). We thus propose that FLVs might lose their capacity over long acclimation to HL (**Fig. 1B**), or long periodicities (**Figs. 2-4**) due to H_2O_2 they produce in the presence of NADPH, which might lead to their degradation (**Fig. S9**). For short timescales of HL or short periodicities of light, FLVs would mostly produce H_2O, remain active, and be a major actor in maintaining the bioenergetic balance. The H_2O_2 produced by FLVs might be a key factor that limits the PCEF bandwidth. If this is the case, that would also open the possibility of it being used by the cell to sense the difference between highly dynamic and less dynamic light environments.

The path for electrons through CMEF is long.

While CMEF was described four decades ago (*22*), its physiological relevance has only been recently highlighted (*13*, *15*, *46*), and the molecular mechanisms involved remain unclear. Here we reveal that CMEF is used under dynamic light conditions, with a bandwidth centered around a periodicity of 10 minutes (**Fig. 2B**), suggesting that the CMEF pathway takes time to shuttle electrons. Amongst the main explored hypotheses on how electrons are shuttled between

organelles is the oxaloacetate-malate shuttle (*26*), which directly translocates malate and oxaloacetate after their reduction or oxidation by malate dehydrogenases (MDH) in either of the organelles (*47*). Interestingly, upon a dark to light transition in *Arabidopsis*, the NAPD-dependent MDH activity oscillates for 5-10 minutes before reaching steady state (*48*). Such timing could be in accord with the bandwidth of CMEF in *Chlamydomonas*. However, it's worth noting that *Arabidopsis,* like all angiosperms, lacks FLVs (*49*, *50*), which might impact the bandwidths of its AEF as compared to *Chlamydomonas*. Indeed, *Arabidopsis* mutants affected in the regulation of MDHs were shown to be sensitive to 1-hour light periodicity (*51*), suggesting a slightly longer bandwidth of CMEF than in *Chlamydomonas*. The relatively long periodicities of CMEF's bandwidth might also reflect the importance of other, less direct, pathways for trafficking reductant between organelles. Such trafficking has recently been shown to involve the triose-phosphate transporter TPT3 in *Chlamydomonas*, which can transport dihydroxyacetone phosphate (DHAP) and the 3-carbon acid, 3-phosphoglycerate (3-PGA) (*52*). Since it requires DHAP to first be produced during the Calvin-Benson-Bassham cycle, it would be a good candidate for a type of CMEF that would be functional for periodicities of dozens of minutes. The systematic analysis of the bandwidth of each potential CMEF effector would reveal which CMEF route electrons take in dynamic environments.

Acclimation to dynamic energetic environments is periodicity-dependent

Most photosynthetic organisms are subject to dynamic light intensities, including diurnal cycles to which bioenergetic mechanisms acclimate thanks to intracellular clocks (*53*). Our results suggest that photosynthetic cells can sense light shifts of sub-hour periodicities and bioenergetically acclimate to them (**Fig. 4**). Like diurnal clock mechanisms that are present across the tree of life, we propose that the periodicity-dependence of bioenergetic mechanisms, including the potential existence of sub-hour clocks, extends beyond non-photosynthetic organisms. While in some cases, like plants and algae, the periodicity comes from external input of light energy (*2*, *17*), it might also stem from dynamic internal energy demand, like in zebrafish embryos, where a 24-minute periodicity of energy dissipation is observed, which parallels the cell cycle activity (*54*). We envision that defining the bandwidth of mechanisms in response to dynamic environments extends beyond bioenergetic balance. The acclimation to dynamic changes in other biotic factors like temperature or nutrient availability might require mechanisms

that are different from continuous environments, each likely with their own bandwidth of physiological importance.

Acknowledgments

The writing of this manuscript was assisted by Grammarly to improve readability, language, and clarity. The authors keep all accountability for the accuracy and integrity of any part of the present work. The authors thank constructive comments from all members of the Burlacot laboratory. The authors thank Çağla Aybar and Maia Lopin for helping with the initial acquisition of chlorophyll fluorescence data.

Funding

This work was supported by Carnegie Science (A.B.). This work was also partly supported by DOE award DE-SC0019417 (A.B.). L.A. was supported by the Stanford Energy Postdoctoral Fellowship.

Materials and Methods

Growth and culture conditions:

Existing *Chlamydomonas* mutants impaired in each AEF have been generated in different genetic backgrounds (*21*, *23*, *25*, *30*, *46*, *55*), making comparisons of the importance of each pathway in various environments complicated (*15*, *46*). *Chlamydomonas* CC125 and *pgrl1-1* and *pgrl1-2* single mutants were already described in (*56*); all other *pgrl1*, *flvB*, and *pgrl1 flvB* double mutants were produced using CRISPR-Cas9 for this study. All strains developed in this study are available at the Chlamydomonas ressource center (https://www.chlamycollection.org/) (their reference number can be found in **Table S1**) All strains were grown photoautotrophically in 125-mL flasks with cotton stoppers at 25°C in a buffered minimal medium (20 mM MOPS pH 7.2) under constant illumination (50 µmol photons $m^{-2}s^{-1}$, light spectrum shown in **Fig. S10A**) and shaking (120 rpm), either under ambient CO_2 or 2% CO_2 in air. Cells were diluted at least twice before experimentation to ensure active growing and were subsequently sampled at a concentration between 5 to 7 µg Chl mL^{-1}. Throughout the manuscript, a "biologically

independent experiment" refers to a replication done with a fresh new liquid culture of the strains described, seeded from a source culture, and diluted at least twice before the experiment.

For characterizations of PCEF and CMEF performed in **Fig. 4** and **Figs. S8, S9**, cells were cultured in buffered minimal medium and diluted to 1 μg Chl mL^{-1} at 5 pm the day before the experiment. On the day of the experiment, 30 mL was added to a 75 cm² U-shape cell culture flask with a canted neck and placed in the treatment condition (light spectrum shown in **Fig. S10C**). Cells were treated for a total dosage of 4 hours of 100 µmol photons $m^{-2}s^{-1}$ of light under the different light treatments as follows: 4 hours of constant 100 µmol photons $m^{-2}s^{-1}$ (HL) and 8 hours of constant 50 µmol photons $m^{-2}s^{-1}$; for HL/darkness fluctuations, 6 hours of the 2h periodicity, 7.5 h of 30 minutes periodicity and 8 hours of 5 minutes, 1 minute and 30 seconds periodicities. Samples for immunodetection and gas exchange measurements were taken at time zero and at the end of each treatment.

Generation of mutants in the CC125 background:

Chlamydomonas mutants showing targeted insertion in the *FLVB*, the *PGRL1,* or both loci were generated in the CC125 background (mt+, nit-) or single mutants background (mt+, nit-) using CRISPR/Cas-9 targeted mutagenesis (**Table S1**). Single guide RNAs (sgRNAs) (**Table S2**) were designed by CHOPCHOP (1) using version 5.6 of the *Chlamydomonas reinhardtii* genome. Ribonucleic proteins (RNPs) were prepared by duplexing the sgRNA (20% volume per volume - v/v-) and Cas-9 (IDT, Ref# 427093062) (20% v/v) with duplex buffer (IDT, Ref# 325470395) (60% v/v). Before electroporation, cells were grown in Tris-acetate-phosphate (TAP) at 22 °C under continuous illumination of 50 µmol photons $m^{-2}s^{-1}$. After treatment with autolysin for 3 hours, cells were electroporated in the presence of a hygromycin resistance cassette (2 µg mL^{-1}) for the generation of single mutants, or with a paromomycin resistance (2 µg mL^{-1}) cassette for the generation of *pgrl1 flvB* double mutants, and the RNP mixture. The cells were resuspended in 10 mL TAP with 40 mM sucrose and left shaking overnight in dim light (10-20 µmol photons m^{-2} s^{-1}). Hygromycin-resistant or paromomycin-resistant transformants were selected on solid TAP media (2% w/v Agar) containing hygromycin (20 µg mL^{-1}) or paromomycin (20 µg mL^{-1}), respectively. sgRNA-targeted regions were amplified via PCR to check for full or partial insertion of the resistance cassette at the target site (**Table S3 and Fig. S1**).

Growth test:

The different *Chlamydomonas* strains were cultivated at an air level of CO_2 under moderate light (50 μmol photons m^{-2} s^{-1}) at 25 °C in minimal medium at pH 7.2. Cells were collected during exponential growth and diluted in fresh minimal medium to 2, 0.5, and 0.1 µg Chl mL^{-1}. Seven-microliter drops were spotted on 2.0% Agar plates of minimal medium (buffered with 20 mM MOPS pH 7.2) with or without myxothyazol (2.5 μM final concentration) and exposed to air enriched with 2.5% CO_2. Homogeneous light was supplied by LED panels (light spectrum shown in **Fig. S10B**); the different light fluctuation periodicities were obtained with power outlet controllers. The temperature was maintained at 22 °C at the level of the plates. Cells were left to grow for a duration of 5 to 20 days.

Gas exchange measurements:

Gas exchange rates were measured using a membrane inlet mass spectrometer (MIMS)(*57*). Cells acclimated to the different light conditions were collected by centrifugation at 450 × *g* for 3 min and resuspended in 1.5 mL of fresh buffered minimal medium (pH 7.2) at around 25 μg chlorophyll mL^{-1}. HCO_3^- was subsequently added to the cell suspension (10 mM final concentration). The cell suspension was then placed in the MIMS reaction vessel (mounted with a 1 mil Teflon membrane), 100 μL of ^{18}O-enriched O_2 (97% ^{18}O Sigma-Aldrich, ref 490474-1L) was bubbled in the suspension. After closing the vessel, gas exchange was recorded during a dark-to-light-to-dark transition (1300 μmol photons m^{-2} s^{-1}; green LEDs picked at 525 nm; Luminus reference PT-121-G-L11-MPK). Light intensity was set to be saturating using weakly absorbed green light for better homogeneity. As previously described, gross and net O_2 exchange were calculated using the MIMS analysis software (*57*). Final chlorophyll concentration was measured at the end of the experiment.

Chlorophyll fluorescence:

To estimate the electron transport rate through PSII in **Fig. 1**, chlorophyll fluorescence was measured using a PAM fluorometer (Dual-PAM 100, Walz GmbH, Germany) with the red measuring head. Detection pulses (10 µmol photons m^{-2} s^{-1} blue light) were supplied to measure fluorescence (F) at a frequency of 20 Hz. Red saturating flashes (8,000 µmol photons m^{-2} s^{-1}, 300 ms, 620 nm) were delivered to measure *F*M (maximal fluorescence yield in the dark-acclimated samples) and *F*M′ (upon actinic light exposure). Fluorescence emission was

detected using a long-pass filter (>700 nm). The operating yield of photosystem II (Y(II)) was calculated as (FM′-F)/FM′, and the electron transport rate (ETR) was calculated as Y(II) x I x a where I is the actinic light intensity and a is a factor correcting for the incident light non absorbed (here we used the machine's default value a = 0.84). The Chl concentration of the sample was ~5–8 µg Chl $ml^{-1,}$ and the sample was bubbled with a custom gas mixture (5% CO_2, 20% O_2, 75% N_2) at a flux of 15 cm^3 min^{-1} for proper control of the gas concentrations of the sample throughout the entire experiment duration. Cells were dark-adapted for ten minutes before starting measurements for light intensity response or light fluctuation treatment, respectively. Light response curves were obtained by incrementally increasing the actinic light intensity every 1 minute (**Fig. 1, Fig. S2**).

To estimate the electron transport rate through PSII in **Fig. 3**, chlorophyll fluorescence was measured using a PAM camera fluorometer (Maxi-PAM, Walz GmbH, Germany) with red measuring LEDs. Cells were grown in flasks and transferred to 24-well plates for the light treatment, after which they were put under the camera for measurement. Cells were dark-adapted for five minutes prior to measurement. Detection pulses (10 µmol photons m^{-2} s^{-1} red light) were supplied to measure fluorescence (F) at 2 Hz. Red saturating flashes (8,000 µmol photons m^{-2} s^{-1}, 300 ms, 620 nm) were delivered to measure FM (maximal fluorescence yield in the dark-acclimated samples) and FM′ (upon actinic light exposure). Fluorescence emission was detected using a long-pass filter (>700 nm). The operating yield of photosystem II (Y(II)) was calculated as (FM′-F)/FM′ and was measured after three minutes of 12 µmol photons $m^{-2}s^{-1}$. The Chl concentration of the sample was between 3 to 5 µg Chl $ml^{-1,}$ and the sample was spiked with 0.5 mM bicarbonate (final concentration) to avoid carbon limitation during the measurement.

Protein extraction, SDS PAGE, and Immunoblotting:

Cells were collected by centrifugation at 1,000 g for 5 minutes at room temperature, and cell pellets were stored at -80℃. Total protein was extracted by homogenizing the cell pellet in a solution comprising 1% SDS, 50 mM DTT, 1 mM Aminocaproic acid, and 1 mM benzamidine hydrochloride, with buffering by 60 mM Tris (pH 6.8) and heating at 100°C for one minute. The resulting cell lysate was centrifuged (10,000 g; 5 minutes), and the supernatant was incubated with acetone (80% final concentration) at -20°C for 1 hour. Proteins were subsequently pelleted

by centrifugation (5,000 g; 5 minutes) and resuspended in a storage buffer containing 1% SDS, with 60 mM Tris (pH 6.8). Protein concentration was estimated utilizing the Microplate BCA protein assay Kit (compatible with reducing agents, Thermo Scientific), with bovine serum albumin as the standard. For subsequent analysis, protein extracts (10 µg protein) were loaded onto a 12% SDS-PAGE gel, running for 1 hour at 150V in Tris-glycine SDS buffer alongside the Precision Plus Protein Dual Color Standards molecular ladder (Biorad). The proteins were then transferred to a nitrocellulose membrane using a semi-dry transfer system (Transblot turbo, Biorad). Immunoblot detection featured antibodies against FlvB (1:1,000)(*21*), FlvA (1:500) (*21*), and PGRL1 (1:1,000) (*25*), and other antibodies PsbA (1:10000) (AS05 084), PsaA (1:3000) (AS06 172), H3 Histone (1:5000) (AS10 710), AOX1 (1:10,000) (AS06 152) and COXIIB (1:10,000) (AS06 151) were procured from Agrisera (https://www.agrisera.com/). An anti-rabbit HRP-conjugated antibody (1:25,000) (AS09 602) was employed as a secondary antibody for immunodetection.

Accession numbers

Genes studied in this article can be found on https://phytozome-next.jgi.doe.gov/ under the loci Cre12.g531900 (*FLVA*), Cre16.g691800 (*FLVB*), and Cre07.g340200 (*PGRL1*).

Figures Legends

Figure 1. Each AEF's capacity to maintain algal bioenergetic homeostasis in response to light widely differs. (**A**) Schematic representation of the major photosynthetic electron transport systems in the green microalgae *Chlamydomonas*. Linear electron flow (LEF, gray arrow) drives the production of NADPH and generates a trans-thylakoidal proton (H^+) gradient utilized for ATP synthesis. Both NADPH and ATP fuel cell's metabolism. Cyclic electron flow (CEF, blue arrow) and pseudo-cyclic electron flow (PCEF, green arrow) rebalance ATP generation and NADPH amounts within the chloroplast. The chloroplast-to-mitochondria electron flow (CMEF, purple arrow) allows the transformation of chloroplastic reductant into ATP mostly via the complex III/IV pathway. (**B**) Growth tests for *pgrl1, flvB, pgrl1 flvB* double mutant, and their corresponding control strains (WT) in the presence (+myxo) or absence (control) of the mitochondrial complex III inhibitor myxothiazol (2.5 μM final concentration). Cells were spotted at various initial chlorophyll concentration on plates containing minimal medium at pH 7.2 and grown under continuous low light (LL, 25 μmol photon m^{-2} s^{-1} for 6 days), medium light (ML, 50 μmol photon m^{-2} s^{-1} for 6 days), or high light (HL, 100 μmol photon m^{-2} s^{-1} for 4 days) in air enriched at 2% CO_2. Spots shown are representative of n=10 biologically independent experiments. (**C**) Relative PSII electron transport rate (ETR) sustained by each individual AEF after 1 minute of illumination at different light intensities. Plain lines show the average, and dots show single replicates (n = 3 biologically independent samples).

Figure 2. Each AEF harbors a specific bandwidth for sustaining the cell's bioenergetic homeostasis in dynamic environments. (**A**) Illustration of the type of fluctuating light patterns used. Illustrated is a fluctuating light with a periodicity of 10 min. (**B**) Quantification of the growth capacity relative to the WT levels when only one of the main AEFs is active. Shown are greenness levels relative to the WT for the first two dilutions of spots shown in **Figs. S4, S5.** Plain lines connect averages, and dots represent individual replicates (n = 2 technical replicates for each n = 3 biologically independent samples). Note that replicates from *pgrl1-2* are not shown here as this strain showed a stronger general sensitivity to light, independent of light periodicity, which was not linked to the *pgrl1* mutation (**Figs. S4, S5**). Shown at a periodicity of 1000 minutes is continuous HL.

Figure 3. CMEF and PCEF capacity to sustain photosynthetic electron flow follows a similar behavior to their bandwidth. Maximal PSII activity (Fv/Fm; top panels) and PSII electron transport rate (ETR; bottom panels) sustained by CMEF (**A**) or PCEF (**B**) relative to the wildtype under various light periodicities after receiving photon number equivalent to 4 hours of continuous high light (100 μmol photon m^{-2} s^{-1}). Plain lines show the average, and dots show single replicates (n = 3 biologically independent samples). Shown at a periodicity of 1000 minutes is after 4 hours of continuous HL.

Figure 4. PCEF and CMEF activities in WT cells parallel their bandwidth. Gas exchange rates were measured in wildtype cells after receiving a number of photons equivalent to 4 hours of continuous high light (100 μmol photon m^{-2} s^{-1}) for a range of light periodicities. (A, B) Gross O_2 uptake at the onset of a dark-to-light transition (A, related to PCEF activity) or in the dark (B, related to CMEF) after cells' acclimation to a range of light periodicities. Plain lines show the average, and dots show single replicates (n = 3 biologically independent samples). Shown at a periodicity of 1000 minutes is after 4 hours of continuous HL.

References

1. D. C. Wallace, Bioenergetics, the origins of complexity, and the ascent of man. *Proc. Natl. Acad. Sci.* **107**, 8947–8953 (2010).

2. R. A. Slattery, B. J. Walker, A. P. M. Weber, D. R. Ort, The impacts of fluctuating light on crop performance. *Plant Physiol.* **176**, 990–1003 (2017).

3. R. Putti, R. Sica, V. Migliaccio, L. Lionetti, Diet impact on mitochondrial bioenergetics and dynamics. *Front. Physiol.* **6** (2015).

4. A. Bratic, N.-G. Larsson, The role of mitochondria in aging. *J. Clin. Invest.* **123**, 951–957 (2013).

5. S. B. Vafai, V. K. Mootha, Mitochondrial disorders as windows into an ancient organelle. *Nature* **491**, 374–383 (2012).

6. D. C. Chan, Mitochondrial Dynamics and Its Involvement in Disease. *Annu. Rev. Pathol. Mech. Dis.* **15**, 235–259 (2020).

7. E. Fernandez-Vizarra, M. Zeviani, Mitochondrial disorders of the OXPHOS system. *FEBS Lett.* **595**, 1062–1106 (2021).

8. C. Tomas, A. Brown, V. Strassheim, J. Elson, J. Newton, P. Manning, Cellular bioenergetics is impaired in patients with chronic fatigue syndrome. *PLOS ONE* **12**, e0186802 (2017).

9. B. D. Paul, M. D. Lemle, A. L. Komaroff, S. H. Snyder, Redox imbalance links COVID-19 and myalgic encephalomyelitis/chronic fatigue syndrome. *Proc. Natl. Acad. Sci.* **118**, e2024358118 (2021).

10. A. Zuin, N. Gabrielli, I. A. Calvo, S. García-Santamarina, K.-L. Hoe, D. U. Kim, H.-O. Park, J. Hayles, J. Ayté, E. Hidalgo, Mitochondrial Dysfunction Increases Oxidative Stress and Decreases Chronological Life Span in Fission Yeast. *PLOS ONE* **3**, e2842 (2008).

11. S. L. Rea, N. Ventura, T. E. Johnson, Relationship Between Mitochondrial Electron Transport Chain Dysfunction, Development, and Life Extension in Caenorhabditis elegans. *PLOS Biol.* **5**, e259 (2007).

12. Y. Munekage, M. Hashimoto, C. Miyake, K.-I. Tomizawa, T. Endo, M. Tasaka, T. Shikanai, Cyclic electron flow around photosystem I is essential for photosynthesis. *Nature* **429**, 579–582 (2004).

13. A. M. Vera-Vives, P. Novel, K. Zheng, S. Tan, M. Schwarzländer, A. Alboresi, T. Morosinotto, Mitochondrial respiration is essential for photosynthesis-dependent ATP supply of the plant cytosol. *New Phytol.* **243**, 2175–2186 (2024).

14. P. Cardol, J. Alric, J. Girard-Bascou, F. Franck, F. A. Wollman, G. Finazzi, Impaired respiration discloses the physiological significance of state transitions in *Chlamydomonas*. *Proc. Natl. Acad. Sci. U. S. A.* **106**, 15979–15984 (2009).

15. G. Peltier, C. Stoffel, J. Findinier, S. K. Madireddi, O. Dao, V. Epting, A. Morin, A. Grossman, Y. Li-Beisson, A. Burlacot, Alternative electron pathways of photosynthesis power green algal CO_2 capture. *Plant Cell*, koae143 (2024).

17. N. A. Eckardt, Y. Allahverdiyeva, C. E. Alvarez, C. Büchel, A. Burlacot, T. Cardona, E. Chaloner, B. D. Engel, A. R. Grossman, D. Harris, N. Herrmann, M. Hodges, J. Kern, T. D. Kim, V. G. Maurino, C. W. Mullineaux, H. Mustila, L. Nikkanen, G. Schlau-Cohen, M. A. Tronconi, W. Wietrzynski, V. K. Yachandra, J. Yano, Lighting the way: Compelling open questions in photosynthesis research. *Plant Cell* **36**, 3914–3943 (2024).

18. W. J. Nawrocki, B. Bailleul, D. Picot, P. Cardol, F. Rappaport, F. A. Wollman, P. Joliot, The mechanism of cyclic electron flow. *Biochim. Biophys. Acta BBA - Bioenerg.* **1860**, 433–438 (2019).

19. G. Curien, S. Flori, V. Villanova, L. Magneschi, C. Giustini, G. Forti, M. Matringe, D. Petroutsos, M. Kuntz, G. Finazzi, The Water to Water Cycles in Microalgae. *Plant Cell Physiol.* **57**, 1354–1363 (2016).

20. C. Gerotto, A. Alboresi, A. Meneghesso, M. Jokel, M. Suorsa, E.-M. Aro, T. Morosinotto, Flavodiiron proteins act as safety valve for electrons in Physcomitrella patens. *Proc. Natl. Acad. Sci.* **113**, 12322–12327 (2016).

21. F. Chaux, A. Burlacot, M. Mekhalfi, P. Auroy, S. Blangy, P. Richaud, G. Peltier, Flavodiiron proteins promote fast and transient O_2 photoreduction in Chlamydomonas. *Plant Physiol.* **174**, 1825–1836 (2017).

22. C. Lemaire, F. A. Wollman, P. Bennoun, Restoration of phototrophic growth in a mutant of *Chlamydomonas reinhardtii* in which the chloroplast *atpB* gene of the ATP synthase has a deletion: an example of mitochondria-dependent photosynthesis. *Proc. Natl. Acad. Sci. U. S. A.* **85**, 1344–1348 (1988).

23. P. Cardol, G. Gloire, M. Havaux, C. Remacle, R. Matagne, F. Franck, Photosynthesis and state transitions in mitochondrial mutants of *Chlamydomonas reinhardtii* affected in respiration. *Plant Physiol.* **133**, 2010–2020 (2003).

24. A. Burlacot, Quantifying the roles of algal photosynthetic electron pathways: a milestone towards photosynthetic robustness. *New Phytol.* (2023).

25. D. Tolleter, B. Ghysels, J. Alric, D. Petroutsos, I. Tolstygina, D. Krawietz, T. Happe, P. Auroy, J. M. Adriano, A. Beyly, S. Cuine, J. Plet, I. M. Reiter, B. Genty, L. Cournac, M. Hippler, G. Peltier, Control of hydrogen photoproduction by the proton gradient generated by cyclic electron flow in *Chlamydomonas reinhardtii*. *Plant Cell* **23**, 2619–2630 (2011).

26. O. Dao, F. Kuhnert, A. P. M. Weber, G. Peltier, Y. Li-Beisson, Physiological functions of malate shuttles in plants and algae. *Trends Plant Sci.* **27**, 488–501 (2022).

27. G. Shimakawa, Y. Matsuda, A. Burlacot, Crosstalk between photosynthesis and respiration in microbes. *J. Biosci.* **49**, 45 (2024).

28. K. V. Dang, J. Plet, D. Tolleter, M. Jokel, S. Cuine, P. Carrier, P. Auroy, P. Richaud, X. Johnson, J. Alric, Y. Allahverdiyeva, G. Peltier, Combined increases in mitochondrial cooperation and oxygen photoreduction compensate for deficiency in cyclic electron flow in *Chlamydomonas reinhardtii*. *Plant Cell* **26**, 3036–50 (2014).

29. M. Jokel, X. Johnson, G. Peltier, E.-M. Aro, Y. Allahverdiyeva, Hunting the main player enabling *Chlamydomonas reinhardtii* growth under fluctuating light. *Plant J.* **94**, 822–835 (2018).

30. Y. Kaye, W. Huang, S. Clowez, S. Saroussi, A. Idoine, E. Sanz-Luque, A. R. Grossman, The mitochondrial alternative oxidase from *Chlamydomonas reinhardtii* enables survival in high light. *J. Biol. Chem.* **294**, 1380–1395 (2019).

31. L. Cournac, K. Redding, J. Ravenel, D. Rumeau, E.-M. Josse, M. Kuntz, G. Peltier, Electron flow between photosystem II and oxygen in chloroplasts of photosystem I-deficient algae is mediated by a quinol oxidase involved in chlororespiration. *J. Biol. Chem.* **275**, 17256–17262 (2000).

32. L. Nedbal, V. Březina, Complex Metabolic Oscillations in Plants Forced by Harmonic Irradiance. *Biophys. J.* **83**, 2180–2189 (2002).

33. A. Alboresi, M. Storti, T. Morosinotto, Balancing protection and efficiency in the regulation of photosynthetic electron transport across plant evolution. *New Phytol.* **221**, 105–109 (2019).

34. W. W. Garner, H. A. Allard, Effect of abnormally long and short alternations of light and darkness on growth and development of plants. *J. Agric. Res.* (1931).

35. M. E. Pérez-Pérez, A. Mauriès, A. Maes, N. J. Tourasse, M. Hamon, S. D. Lemaire, C. H. Marchand, The Deep Thioredoxome in Chlamydomonas reinhardtii: New Insights into Redox Regulation. *Mol. Plant* **10**, 1107–1125 (2017).

36. R. J. Radmer, B. Kok, Photoreduction of O_2 pimes and replaces CO_2 assimilation. *Plant Physiol.* **58**, 336–340 (1976).

37. G. Shimakawa, K. Ishizaki, S. Tsukamoto, M. Tanaka, T. Sejima, C. Miyake, The Liverwort, Marchantia, drives alternative electron flow using a flavodiiron protein to protect PSI. *Plant Physiol.* **173**, 1636–1647 (2017).

38. A. Alboresi, M. Storti, L. Cendron, T. Morosinotto, Role and regulation of class-C flavodiiron proteins in photosynthetic organisms. *Biochem. J.* **476**, 2487–2498 (2019).

39. N. Rizzetto, E. Traverso, A. Sabia, F. Fiorin, C. Francese, L. Trainotti, T. Morosinotto, A. Alboresi, Flavodiiron protein activity outcompetes cyclic electron transport when expressed in angiosperm Nicotiana tabacum. bioRxiv [Preprint] (2025). https://doi.org/10.1101/2025.01.23.634494.

40. M. R. A. Blomberg, P. Ädelroth, Reduction of molecular oxygen in flavodiiron proteins -

Catalytic mechanism and comparison to heme-copper oxidases. *J. Inorg. Biochem.* **255**, 112534 (2024).

41. M. C. Martins, C. M. Alves, M. Teixeira, F. Folgosa, The flavodiiron protein from Syntrophomonas wolfei has five domains and acts both as an NADH:O2 or an NADH:H2O2 oxidoreductase. *FEBS J.* **291**, 1275–1294 (2024).

42. P. Sétif, G. Shimakawa, A. Krieger-Liszkay, C. Miyake, Identification of the electron donor to flavodiiron proteins in Synechocystis sp. PCC 6803 by in vivo spectroscopy. *Biochim. Biophys. Acta BBA - Bioenerg.* **1861**, 148256 (2020).

43. C. Beraldo, E. Traverso, M. Boschin, L. Cendron, T. Morosinotto, A. Alboresi, Physcomitrium patens flavodiiron proteins form heterotetrametric complexes. *J. Biol. Chem.* **300** (2024).

44. J. H. Jang, D. B. Kim, Y. Choi, R. Amir, D.-E. Cheong, H.-J. Chung, S.-H. Ahn, G.-J. Kim, D. W. Lee, O. R. Lee, E.-S. Kim, Real-time monitoring of stromal NADPH levels in Arabidopsis using a metagenome-derived NADPH-binding fluorescent protein. *Plant Physiol. Biochem.* **217**, 109260 (2024).

45. K. Tanaka, G. Shimakawa, H. Tabata, S. Kusama, C. Miyake, S. Nakanishi, Quantification of NAD(P)H in cyanobacterial cells by a phenol extraction method. *Photosynth. Res.* **148**, 57–66 (2021).

46. A. Burlacot, O. Dao, P. Auroy, S. Cuiné, Y. Li-Beisson, G. Peltier, Alternative photosynthesis pathways drive the algal CO_2 concentrating mechanism. *Nature*, doi: https://doi.org/10.1038/s41586-022-04662-9 (2022).

47. J. Selinski, R. Scheibe, Malate valves: old shuttles with new perspectives. *Plant Biol*, doi: https://doi.org/10.1111/plb.12869 (2018).

48. R. Scheibe, M. Stitt, Comparison of Nadp-Malate Dehydrogenase Activation, Qa Reduction and O-2 Evolution in Spinach Leaves. *Plant Physiol. Biochem.* (1988).

49. G. Peltier, D. Tolleter, E. Billon, L. Cournac, Auxiliary electron transport pathways in chloroplasts of microalgae. *Photosynth. Res.* **106**, 19–31 (2010).

50. H. Yamamoto, S. Takahashi, M. R. Badger, T. Shikanai, Artificial remodelling of alternative electron flow by flavodiiron proteins in Arabidopsis. *Nat. Plants* **2**, 16012 (2016).

51. Y. Yokochi, K. Yoshida, F. Hahn, A. Miyagi, K. Wakabayashi, M. Kawai-Yamada, A. P. M. Weber, T. Hisabori, Redox regulation of NADP-malate dehydrogenase is vital for land plants under fluctuating light environment. *Proc. Natl. Acad. Sci.* **118**, e2016903118 (2021).

52. W. Huang, A. Krishnan, A. Plett, M. Meagher, N. Linka, Y. Wang, B. Ren, J. Findinier, P. Redekop, N. Fakhimi, R. G. Kim, D. A. Karns, N. Boyle, M. C. Posewitz, A. R. Grossman, Chlamydomonas mutants lacking chloroplast TRIOSE PHOSPHATE TRANSPORTER3

are metabolically compromised and light-sensitive. *Plant Cell*, koad095 (2023).

53. D. Bell-Pedersen, V. M. Cassone, D. J. Earnest, S. S. Golden, P. E. Hardin, T. L. Thomas, M. J. Zoran, Circadian rhythms from multiple oscillators: lessons from diverse organisms. *Nat. Rev. Genet.* **6**, 544–556 (2005).

54. J. Rodenfels, K. M. Neugebauer, J. Howard, Heat Oscillations Driven by the Embryonic Cell Cycle Reveal the Energetic Costs of Signaling. *Dev. Cell* **48**, 646-658.e6 (2019).

55. X. Johnson, J. Steinbeck, R. M. Dent, H. Takahashi, P. Richaud, S. I. Ozawa, L. Houille-Vernes, D. Petroutsos, F. Rappaport, A. R. Grossman, K. K. Niyogi, M. Hippler, J. Alric, Proton Gradient Regulation 5-mediated cyclic electron flow under ATP- or redox-limited conditions: A study of Δ*ATPase pgr5* and *ΔrbcL pgr5* mutants in the green alga *Chlamydomonas reinhardtii*. *Plant Physiol.* **165**, 438–452 (2014).

56. O. Dao, A. Burlacot, F. Buchert, M. Bertrand, P. Auroy, C. Stoffel, S. K. Madireddi, J. Irby, M. Hippler, G. Peltier, Y. Li-Beisson, Cyclic and pseudo-cyclic electron pathways play antagonistic roles during nitrogen deficiency in Chlamydomonas reinhardtii. *Plant Physiol.* **197**, kiae617 (2025).

57. A. Burlacot, F. Burlacot, Y. Li-Beisson, G. Peltier, Membrane Inlet Mass Spectrometry: A Powerful Tool for Algal Research. *Front. Plant Sci.* **11** (2020).

Supplemental Tables

Table S1: List of mutants generated in this study, their CC-number at the Chlamydomonas collection (U. Minnesota), and sgRNAs used to knock out target genes

Gene ID mutated	Strains	Genetic background	CC-number	sgRNA
Cre07.g340200 (*PGRL1*)	*pgrl1-1*	CC125	CC-6235	gAB004
	pgrl1-2	CC125	CC-6563	gAB023
	pgrl1-3	CC125	CC-6237	gAB004
	pgrl1-4	CC125	CC-6236	gAB023
Cre16.g691800 (*FLVB*)	*flvB-1*	CC125	CC-6239	gAB002
	flvB-2	CC125	CC-6268	gAB002
Cre07.g340200/Cre16.g691800 (*PGRL1* and *FLVB*)	*pgrl1 flvB-1*	*flvB-1*	CC-6241	gAB002 & gAB023
	pgrl1 flvB-2	*pgrl1-2*	CC-6242	gAB023 & gAB002
	pgrl1 flvB-3	*flvB-1*	CC-6243	gAB002 & gAB004
	pgrl1 flvB-4	*pgrl1-2*	CC-6244	gAB023 & gAB002

Table S2: sgRNAs to knockout target genes

sgRNA name	Gene ID targeted	sgRNA Sequence	Target Exon
gAB004	Cre07.g340200	CTTGCCCTCGTAGTACCACGAGG	1
gAB023	Cre07.g340200	TTCGCCGAGCGCAGAAGCATCGG	1
gAB002	Cre16.g69180	GTTGTGGAATTTCTCGTGGGAGG	5

Table S3: Primer pair sequences for genotyping mutants

Target Gene	sgRNA targeting locus	Primer Name	Oligo Sequences	Predicted Band Size in CC-125 (bp)
Cre07.g340200 (*PGRL1*)	gAB004	oAB0013	GCAATGTTGCTGCTGACTACTG	270
	gAB004	oAB0014	AGTCCTCGTCAGTCATAATGGG	
	gAB023	oAB0101	ATCCTCCCCCGTCTCATCC	514
	gAB023	oAB0102	GGACCAGATCAGCTCCTCCT	
Cre16.g691800(*FLVB*)	gAB002	oAB0005	CGGCTAATTCTTTCTTGCAAAC	244
	gAB002	oAB0006	CATCAAAAACACACACACATGC	
Cre02.g120250 (*STT7*)	Control	oAB0033	GCACGAACCAAGACACACATAG	280
	Control	oAB0034	GTAGACGATGTCACCGCACTT	

Table S4: Growth time for spot tests shown in Fig. S4 and S5 (days)

Periodicity	Control	+myxo
ML	6	5
1 min	14	12
2 min	14	11
10 min	12	11
1h	11	9
4h	11	8
HL	5	5

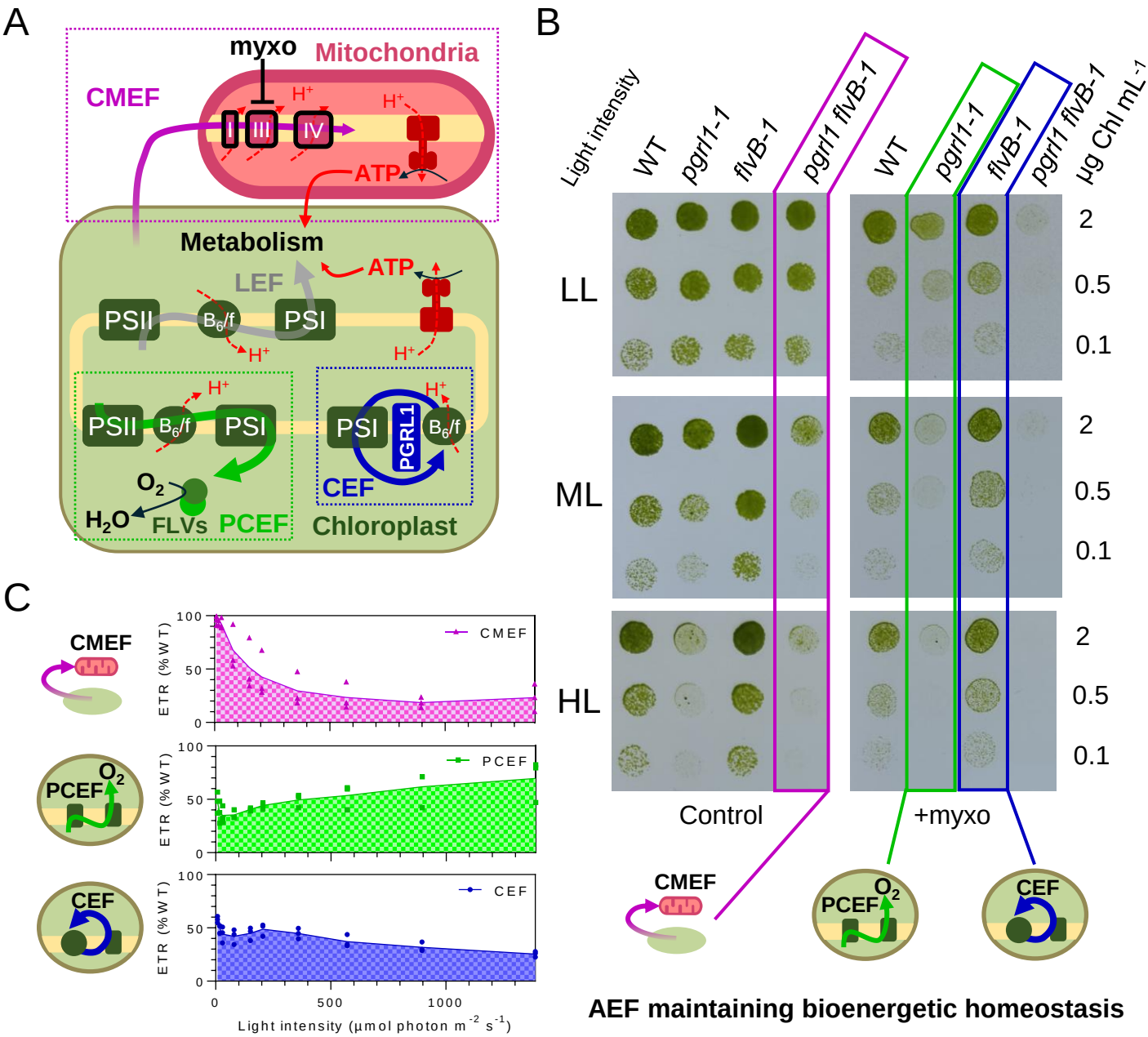

Figure 1. Each AEF's capacity to maintain algal bioenergetic homeostasis in response to light widely differs. (**A**) Schematic representation of the major photosynthetic electron transport systems in the green microalgae *Chlamydomonas*. Linear electron flow (LEF, gray arrow) drives the production of NADPH and generates a trans-thylakoidal proton (H^+) gradient utilized for ATP synthesis. Both NADPH and ATP fuel cell's metabolism. Cyclic electron flow (CEF, blue arrow) and pseudo-cyclic electron flow (PCEF, green arrow) rebalance ATP generation and NADPH amounts within the chloroplast. The chloroplast-to-mitochondria electron flow (CMEF, purple arrow) allows the transformation of chloroplastic reductant into ATP mostly via the complex III/IV pathway. (**B**) Growth tests for *pgrl1, flvB, pgrl1 flvB* double mutant, and their corresponding control strains (WT) in the presence (+myxo) or absence (control) of the mitochondrial complex III inhibitor myxothiazol (2.5 μM final concentration). Cells were spotted at various initial chlorophyll concentration on plates containing minimal medium at pH 7.2 and grown under continuous low light (LL, 25 μmol photon m^{-2} s^{-1} for 6 days), medium light (ML, 50 μmol photon m^{-2} s^{-1} for 6 days), or high light (HL, 100 μmol photon m^{-2} s^{-1} for 4 days) in air enriched at 2% CO_2. Spots shown are representative of n=10 biologically independent experiments. (**C**) Relative PSII electron transport rate (ETR) sustained by each individual AEF after 1 minute of illumination at different light intensities. Plain lines show the average, and dots show single replicates (n = 3 biologically independent samples).

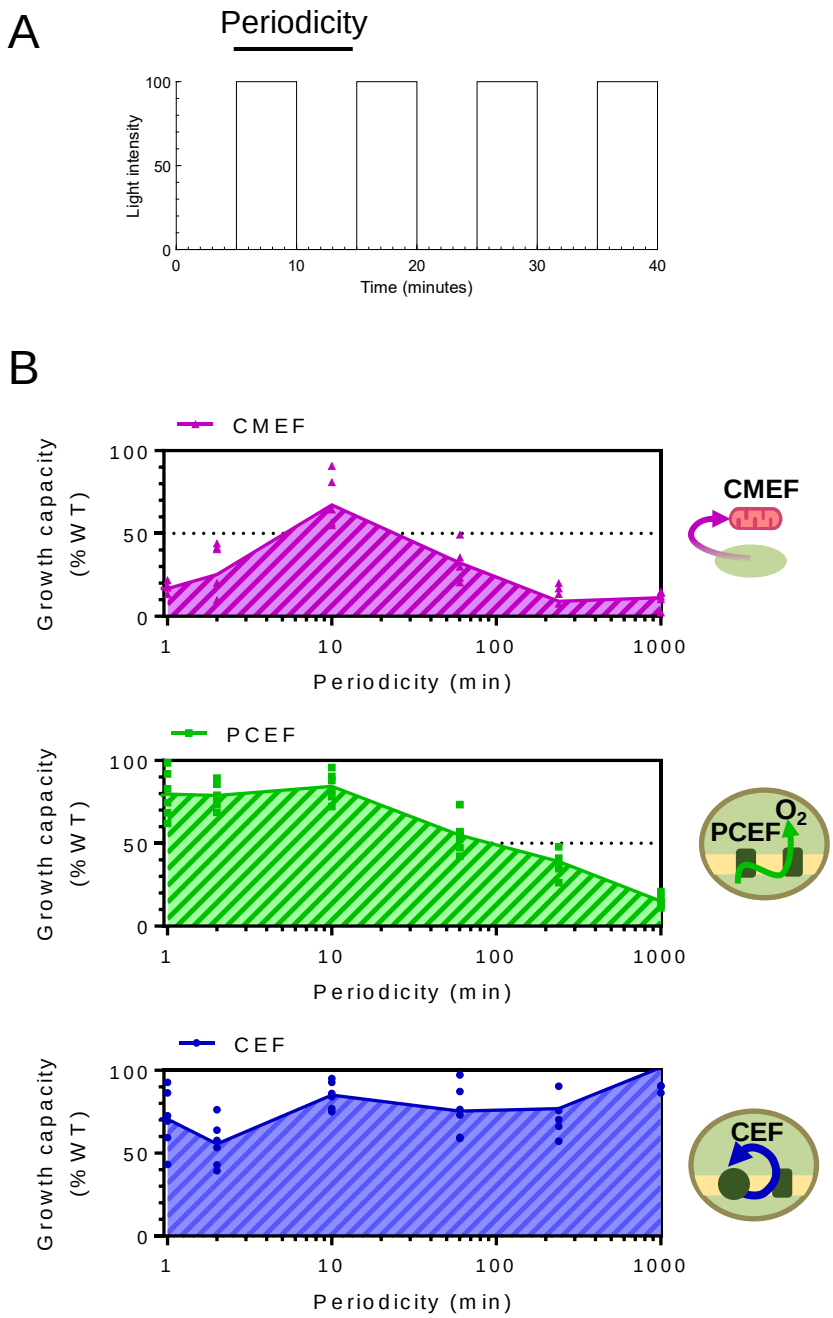

Figure 2. Each AEF harbors a specific bandwidth for sustaining the cell's bioenergetic homeostasis in dynamic environments. (**A**) Illustration of the type of fluctuating light patterns used. Illustrated is a fluctuating light with a periodicity of 10 min. (**B**) Quantification of the growth capacity relative to the WT levels when only one of the main AEFs is active. Shown are greenness levels relative to the WT for the first two dilutions of spots shown in **Figs. S4, S5.** Plain lines connect averages, and dots represent individual replicates (*n* = 2 technical replicates for each *n* = 3 biologically independent samples). Note that replicates from *pgrl1-2* are not shown here as this strain showed a stronger general sensitivity to light, independent of light periodicity, which was not linked to the *pgrl1* mutation (**Figs. S4, S5**). Shown at a periodicity of 1000 minutes is continuous HL.

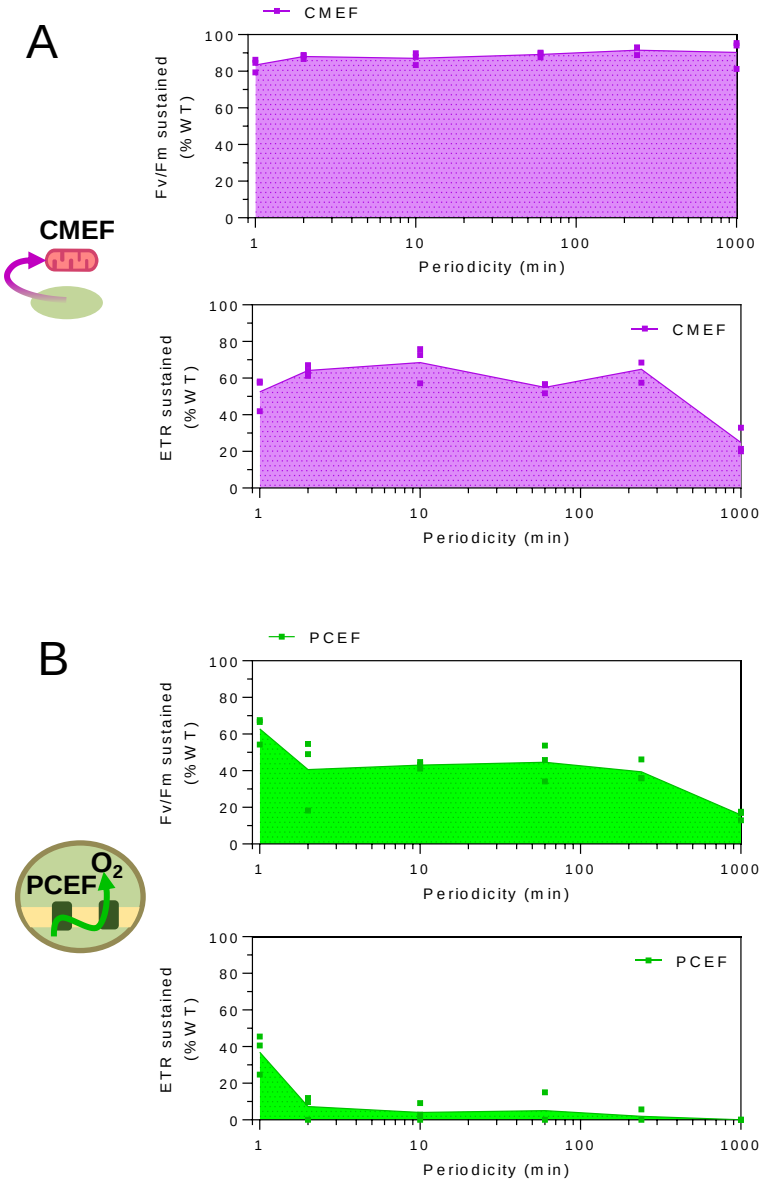

Figure 3. CMEF and PCEF capacity to sustain photosynthetic electron flow follows a similar behavior to their bandwidth. Maximal PSII activity (Fv/Fm; top panels) and PSII electron transport rate (ETR; bottom panels) sustained by CMEF (**A**) or PCEF (**B**) relative to the wildtype under various light periodicities after receiving photon number equivalent to 4 hours of continuous high light (100 μmol photon m^{-2} s^{-1}). Plain lines show the average, and dots show single replicates (n = 3 biologically independent samples). Shown at a periodicity of 1000 minutes is after 4 hours of continuous HL.

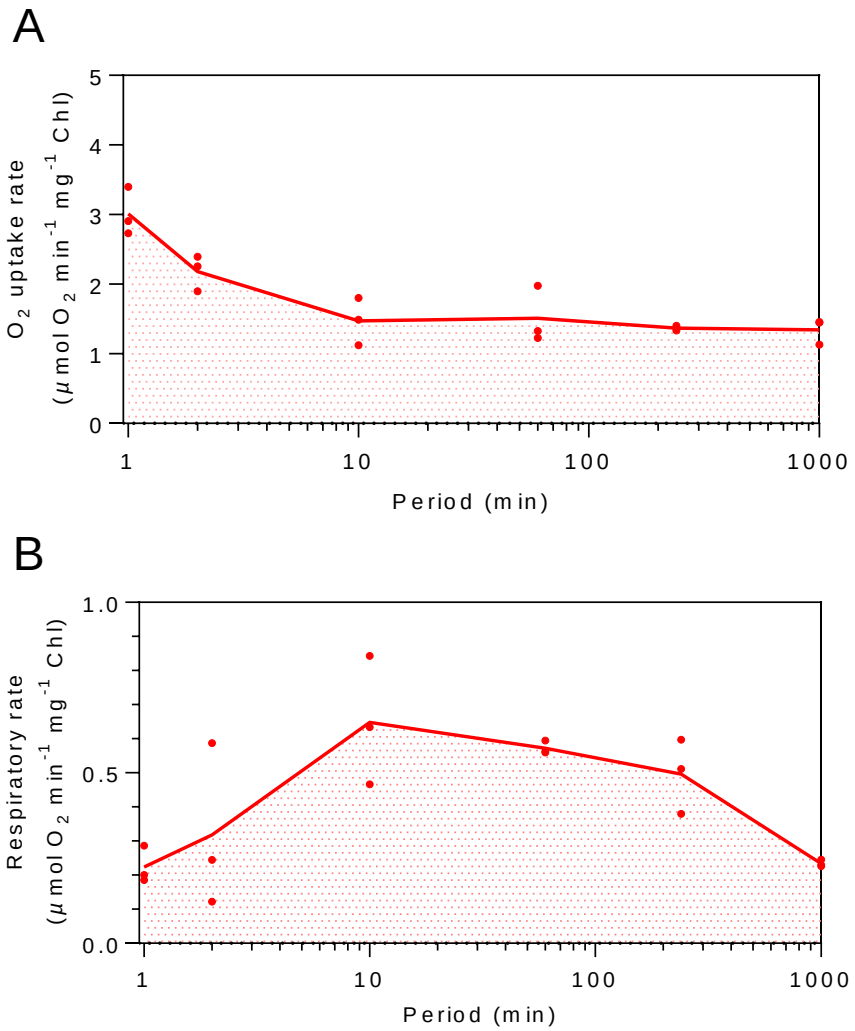

Figure 4. PCEF and CMEF activities in WT cells parallel their bandwidth. Gas exchange rates were measured in wildtype cells after receiving a number of photons equivalent to 4 hours of continuous high light (100 μmol photon m^{-2} s^{-1}) for a range of light periodicities. (**A, B**) Gross O_2 uptake at the onset of a dark-to-light transition (**A**, related to PCEF activity) or in the dark (**B**, related to CMEF) after cells' acclimation to a range of light periodicities. Plain lines show the average, and dots show single replicates (n = 3 biologically independent samples). Shown at a periodicity of 1000 minutes is after 4 hours of continuous HL.